JOURNAL OF MECHANICS OF CONTINUA AND MATHEMATICAL SCIENCES
www.journalimcms.org

ISSN (Online) : 2454 -7190 Vol.-21, No.-09, September (2026) pp 156-183 ISSN (Print) 0973-8975

A GENOCCHI WAVELET METHOD FOR HIGHLY OSCILLATORY INTEGRALS WITH AN ENDPOINT SINGULARITY

Umesha V.[1], B. K. Divyashree[2], S. Padmanabhan[3]

[1,2] Department of Mathematics, BMS College of Engineering, Bengaluru, India-560019.

[3]Department of CSE(AI&ML), RNS Institute of Technology, Bengaluru, India-560098.

Email: [1]umesha.maths@bmsce.ac.in, [2]divyashree.maths@bmsce.ac.in, [3]padmanabhan@rnsit.ac.in.

Corresponding Author: **Umesha V.**

https://doi.org/10.26782/jmcms.2026.09.00009

(Received: June 29, 2026; Revised: September 03, 2026; Accepted: September 14, 2026)

Abstract

This study introduces an efficient high-order wavelet quadrature technique for computing highly oscillatory integrals affected by endpoint singular behavior of the form:

$$\int_0^1 f(x)sin\left(\frac{\omega}{x^r}\right)\,dx \;\; and \;\; \int_0^1 f(x)cos\left(\frac{\omega}{x^r}\right)\,dx, \omega \gg 1, r > 0,$$

where standard numerical methods often lose stability and accuracy due to infinite oscillation frequency as $x \to 0^+$*. The method applies sixth-order Genocchi wavelets within a multiresolution structure to approximate the smooth component of the integrand, while the singular boundary region is treated separately using analytical asymptotic approximations and interval decomposition. Closed-form expressions for the oscillatory kernels are obtained through appropriate transformations. Tests on several benchmark examples demonstrate very high precision, with errors ranging from* 10^{-9}*to* 10^{-13}*, and show clear improvements in both accuracy and efficiency compared to existing wavelet and hybrid approaches. A practical application to radar cross-section computation is presented.*

Keywords: Highly oscillatory integrals, Genocchi wavelets, singular oscillations, numerical integration, adaptive resolution.

I. Introduction

Numerical integration of oscillatory functions constitutes a fundamental challenge in scientific computing and arises in a wide spectrum of engineering and physical applications, including Fourier and Laplace transforms, signal processing, wireless communications, image reconstruction, fluid mechanics, electrodynamics, plasma physics, and quantum mechanics [I], [II]. In such applications, the integrands often contain rapidly oscillating trigonometric or exponential kernels, making their numerical evaluation highly sensitive to discretization strategies. Accurate and efficient computation of these integrals is essential for the reliable simulation and analysis of complex real-world phenomena.

Highly oscillatory integrals commonly appear in the general form:

$$\int_a^b f(x)e^{\{i\omega g(x)\}}\,dx \tag{1}$$

or in equivalent real-valued representations involving sine and cosine functions. Here, *f(x)* is a sufficiently smooth amplitude function, *g(x)* is a real-valued phase function, and ω denotes a large oscillatory parameter. As ω increases, severe cancellation effects occur, and classical quadrature methods such as the trapezoidal rule, Simpson's rule, and Gauss–Legendre quadrature fail to deliver accurate results unless extremely fine meshes are employed [III], [IV], [V]. This significantly increases computational cost and can lead to numerical instability.

To overcome these limitations, a variety of numerical techniques have been developed. Filon-type quadrature methods represent one of the earliest systematic approaches for oscillatory integrals, wherein the oscillatory kernel is treated analytically while approximating the slowly varying part of the integrand [VI]. Asymptotic methods such as the method of stationary phase and steepest descent have also been extensively studied for integrals involving large frequency parameters [III], [IV], [V], [VI], [VII]. In addition, generalized Gaussian quadrature rules and Gauss–Legendre-based techniques have been proposed for oscillatory integrals in one and higher dimensions [VIII], [IX].

More recently, wavelet-based and hybrid numerical schemes have gained considerable attention due to their localization properties and flexibility [X], [XI]. Aziz *et al.* proposed quadrature rules based on Haar wavelets and hybrid functions for numerical integration [XII], while Siraj-ul-Islam and co-authors developed wavelet-based methods for multidimensional highly oscillatory and non-oscillatory integrals [XIII]. New quadrature rules for oscillatory integrals with stationary points were introduced in [XIV], demonstrating improved accuracy for challenging oscillatory kernels. Despite these advances, the numerical treatment of oscillatory integrals remains difficult when singular behavior is present.

A particularly challenging class of problems involves oscillatory integrals with singular oscillations at the origin, such as

$$\int_0^1 \mathrm{f(x)}\sin\left(\frac{\omega}{x^r}\right)\,\mathrm{dx}\ \text{ and }\ \int_0^1 \mathrm{f(x)}\cos\left(\frac{\omega}{x^r}\right)\,\mathrm{dx} \tag{2}$$

where *f(x)* is smooth on $(0,1]$ and $\omega > 0, r > 0$ are real parameters. As $x \to 0$, the oscillations become infinitely rapid, introducing a strong singularity in the phase function. Such integrals arise in wave propagation, diffraction theory, high-frequency scattering, and signal analysis. The combined presence of singularity and rapid oscillation severely limits the applicability of standard quadrature schemes.

Several numerical approaches have been proposed to address singular oscillatory integrals, including variable transformation techniques, adaptive quadrature methods, and modified Levin-type schemes [I], [II]. While suitable transformations may reduce the severity of the singularity, the resulting integrals often remain highly oscillatory, necessitating advanced numerical approximation tools. Consequently, there is an ongoing demand for robust methods that can efficiently handle both singular behavior and rapid oscillations.

In parallel, significant progress has been made in polynomial- and wavelet-based numerical methods, particularly in the context of fractional calculus and fractional differential equations (FDEs). Fractional calculus generalizes classical differentiation and integration to non-integer orders and has proven effective in modelling systems with memory and hereditary properties [XV], [XVI], [XVII], [XVIII]. Due to the analytical complexity of FDEs, numerous numerical methods based on collocation techniques, operational matrices, and spectral approximations have been developed [XIX].

Among these approaches, Genocchi polynomials and their associated wavelets have emerged as powerful tools for numerical computation. Genocchi-based techniques have been successfully applied to the numerical solution of nonlinear fractional differential equations, delay systems, and boundary value problems due to their simple analytical structure, sparse operational matrices, and strong approximation properties [XXIV], [XXV]. The localization capability of Genocchi wavelets makes them particularly suitable for problems involving sharp gradients, localized irregularities, and singular behavior.

Motivated by these developments, this paper proposes a novel quadrature framework based on Genocchi wavelets for the numerical integration of highly oscillatory functions with singular oscillations at the origin. The proposed method employs an appropriate variable transformation to regularize the singular oscillatory kernel, followed by a Genocchi wavelet approximation of the smooth part of the integrand. The resulting formulation leads to a sparse system of algebraic equations obtained via collocation, enabling efficient numerical implementation with reduced computational cost.

The proposed Genocchi wavelet-based quadrature scheme offers several advantages. It achieves high accuracy even for large oscillatory parameters, effectively captures localized singular behavior near the origin, and produces sparse algebraic systems that enhance numerical stability and efficiency. Furthermore, the method is straightforward to implement and can be extended to a wide class of oscillatory integrals encountered in applied mathematics and engineering.

Numerical experiments are presented to illustrate the accuracy, robustness, and efficiency of the proposed approach in comparison with existing numerical integration techniques. The results confirm that the Genocchi wavelet-based method provides a reliable and efficient computational framework for evaluating highly oscillatory integrals with singular behavior at the origin.

To the best of the authors' knowledge, this work represents the first systematic application of Genocchi wavelets to the numerical integration of highly oscillatory functions exhibiting singular oscillations at the origin, thereby extending Genocchi-based numerical techniques beyond fractional differential equations to challenging oscillatory integration problems.

II. Mathematical Formulations

Problem Statement

We consider the numerical evaluation of:

$$I_s = \int_0^1 \mathrm{f(x)} \sin\left(\frac{\omega}{x^r}\right) \ \mathrm{dx}, \ I_c = \int_0^1 \mathrm{f(x)} \cos\left(\frac{\omega}{x^r}\right) \ \mathrm{dx} \tag{3}$$

Where:

- $r > 0$ is a real parameter
- $\omega \in R$ is the oscillation parameter (typically large)
- $f: [0,1] \ \rightarrow R$ is assumed smooth or piecewise smooth

The oscillator $\psi_\omega(x) = \sin \omega(x) = \sin\left(\frac{\omega}{x^r}\right) (or\ \psi_\omega(x) = \cos \omega(x) = \cos\left(\frac{\omega}{x^r}\right)$ has frequency $\frac{\omega r}{x^{r+1}}$, which diverges as $x \rightarrow 0^+$. This singularity distinguishes our problem from standard highly oscillatory integrals.

Genocchi Wavelets of Order 6

Genocchi polynomials $\mathrm{G_n(x)}$ are related to Bernoulli and Euler polynomials. The first six Genocchi polynomials (unnormalized) on $[0,1]$ are:

$$\begin{aligned} &G_1(t) = 1, \\ &G_2(t) = 2\mathrm{t} - 1, \\ &\mathrm{G_3(t)} = 6\mathrm{t}^2 - 6\mathrm{t} + 1, \\ &\mathrm{G_4(t)}\ \& = 20\mathrm{t}^3 - 30\mathrm{t}^2 + 12\mathrm{t} - 1, \\ &\mathrm{G_5(t)}\ \& = 70\mathrm{t}^4 - 140\mathrm{t}^3 + 90\mathrm{t}^2 - 20\mathrm{t} + 1, \\ &\mathrm{G_6(t)} = 252\mathrm{t}^5 - 630\mathrm{t}^4 + 560\mathrm{t}^3 - 210\mathrm{t}^2 + 30\mathrm{t} - 1. \end{aligned} \tag{4}$$

These satisfy the orthogonality relation:

$$\int_0^1 \mathrm{G_m(t)G_n(t)dt} = \frac{\delta_{mn}}{2n-1}, m, n = 1,2, \dots ,6. \tag{5}$$

The orthonormal Genocchi polynomials are therefore:

$$\widetilde{G_n(t)} = \sqrt{2n-1} G_n(t), n = 1, \dots ,6. \tag{6}$$

Wavelet Basis Construction

Let $j \geq 0$ be the resolution level, and define $h = 2^{-j}$. Partition $[0,1]$ into 2^j subintervals:

$$I_{j,k} = \left[\frac{k}{2^j}, \frac{k+1}{2^j}\right) = [a_k, b_k), \quad k = 0,1,2, \dots , 2^j - 1, \tag{7}$$

Where $a_k = kh, b_k = (k+1)h.$

On each subinterval, define the local variable $t \in [0,1)$ by:

$$t = \frac{x - a_k}{h} = 2^j x - k. \tag{8}$$

The Genocchi scaling functions at resolution j are:

$$\varphi_{n,k}(x) = \begin{cases} 2^{\frac{j}{2}}\widetilde{G_n}(t), & x \in I_{j,k} \quad n = 1, \dots, 6. \\ 0, & otherwise \end{cases} \tag{9}$$

The approximation space V_j consists of piecewise polynomial functions of degree ≤ 5 on each $I_{j,k}$:

$$V_j = span\{\emptyset_{n,k} : k = 0, \dots, 2^j - 1, n = 1, \dots \dots, 6.\} \tag{10}$$

III. Numerical Method

Wavelet Approximation of $f(x)$

Approximate f(x) by its projection onto (V_j) :

$$f(x) \approx P_j f(x) = \sum_{k=0}^{2^j-1} \sum_{n=1}^{6} c_{\{n,k\}} \emptyset_{\{n,k\}}(x), \tag{11}$$

where the coefficients are:

$$\mathrm{c}_{\{n,k\}} = \langle f, \emptyset_{\{n,k\}} \rangle = \int_{a_k}^{b_k} f(x) \emptyset_{\{n,k\}}(x) dx. \tag{12}$$

Using (8) and (9)

$$c_{\{n,k\}} = h\, 2^{\left\{\frac{j}{2}\right\}} \sqrt{2n-1} \int_0^1 f(a_k + th) G_n(t)\, dt. \tag{13}$$

These integrals are computed using Gaussian quadrature with N_q points (typically $N_q = 10$ is sufficient for smooth f).

Integral Approximation

Substituting (11) into the integrals:

$$I_s \approx \sum_{k=0}^{2^j-1} \sum_{n=1}^{6} c_{\{n,k\}} E^{s}_{\{n,k\}}, \tag{14}$$

$$I_c \approx \sum_{k=0}^{2^j-1} \sum_{n=1}^{6} c_{\{n,k\}} E^{c}_{\{n,k\}}, \tag{15}$$

where the element integrals are:

$$E^{s}_{\{n,k\}} = \int_{a_k}^{b_k} \emptyset_{\{n,k\}}(x) \sin\left(\frac{\omega}{x^r}\right) dx, \tag{16}$$

$$E^{c}_{\{n,k\}} = \int_{a_k}^{b_k} \emptyset_{\{n,k\}}(x) \cos\left(\frac{\omega}{x^r}\right) dx, \tag{17}$$

Computation of Element Integrals

Using the scaling functions $\phi_{\{n,k\}}(x)$ defined in (9) and the element integrals $E^{s}_{\{n,k\}}, E^{c}_{\{n,k\}}$ defined in (16) and (17), we obtain:

$$E^{(s)}_{\{n,k\}} = h\, 2^{j/2} \sqrt{2n-1} \cdot I^{(s)}_{\{n,k\}} \tag{18}$$

$$E^{(c)}_{\{n,k\}} = h\, 2^{j/2} \sqrt{2n-1} \cdot I^{(c)}_{\{n,k\}} \tag{19}$$

where:

$$\mathrm{I}_{\{n,k\}}^{(s)} = \int_0^1 \mathrm{G_n(t)} \sin\left(\frac{\omega}{(a_k+th)^{\mathrm{r}}}\right) dt, \tag{20}$$

$$\mathrm{I}_{\{n,k\}}^{(c)} = \int_0^1 \mathrm{G_n(t)} \cos\left(\frac{\omega}{(a_k+th)^{\mathrm{r}}}\right) dt. \tag{21}$$

We distinguish two cases: $\mathrm{k} = 0$ (singular interval) and $\mathrm{k} \geq 1$ (regular intervals).

Regular Intervals ($\boldsymbol{k} \geq \mathbf{1}$)

For $k \geq 1, a_k > 0$, so $(a_k + th)^{-r}$ is bounded. Let:

$$\xi_k(t) = \frac{\omega}{(a_k+th)^r} \tag{22}$$

The integrals (20) are computed using adaptive oscillatory quadrature. Since $G_n(t)$ is a polynomial of degree $n \leq 5$, we can use a Filon-type approach or Levin's method on each subinterval. Alternatively, for moderate ω, Gaussian quadrature with sufficient points works well.

Singular Interval ($\boldsymbol{k} = \mathbf{0}$)

For $k = 0, a_0 = 0$, and:

$$\xi_0(t) = \frac{\omega}{(th)^r} = \frac{\omega}{h^r t^r} = \Omega t^{-r} \tag{23}$$

where $\Omega = \omega/h^r$.
The integral becomes:

$$I_{n,0}^{(s)} = \int_0^1 G_n(t) \sin(\Omega t^{-r}) dt \tag{24}$$

Asymptotic Validity Condition

The asymptotic expansion in (33) is valid when the following condition holds:

$$\Omega = \frac{\omega}{h^r} > \max\{1, \alpha\}, \text{ where } \alpha = 1 + \frac{m+1}{r} \tag{24a}$$

and m is the polynomial degree index in the expansion (26).
For $\Omega \leq \max\{1, \alpha\}$, the integrals $S(\alpha, \Omega)$ and $C(\alpha, \Omega)$ are computed using:

1. Recurrence relations for $\alpha \in (0,2]$:
$$S(\alpha, a) = \frac{a^{1-\alpha}}{1-\alpha} + \frac{\alpha}{1-\alpha} S(\alpha-2, a), \text{ for } \alpha \neq 1$$
$$C(\alpha, a) = \frac{a^{1-\alpha}}{1-\alpha} + \frac{\alpha}{1-\alpha} C(\alpha-2, a), \text{ for } \alpha \neq 1$$
2. Numerical quadrature of the tail $[\Omega, \Omega + M]$ where M is chosen adaptively such that $|u^{-\alpha} \sin u| < 10^{-15}$ for $u > \Omega + M$
3. Clenshaw-Curtis quadrature for oscillatory integrands with moderate frequency

The transition between asymptotic and numerical regimes is determined automatically based on condition (24a).

Change variables: $u = \Omega t^{-r}$, so $t = (\Omega/u)^{1/r}, dt = -\frac{\Omega^{1/r}}{r} u^{-1-1/r} du$. When $t: 0 \to 1$, $u: \infty \to \Omega$. Thus:

$$I_{n,0}^{(s)} = \frac{\Omega^{1/r}}{r} \int_{\Omega}^{\infty} G_n\left((\Omega/u)^{1/r}\right) \sin(u) u^{-1-1/r} du \quad (25)$$

Let $y = (\Omega/u)^{1/r} = \Omega^{1/r} u^{-1/r}$. Expand $G_n(y)$ as a polynomial:

$$G_n(y) = \sum_{m=0}^{n} b_{n,m} y^m \quad (26)$$

where the coefficients $b_{n,m}$ are derived from (4):

$b_{1,0} = 1,$
$b_{2,0} = -1, b_{2,1} = 2$

$$\begin{aligned} &b_{3,0} = 1, b_{3,1} = -6, b_{3,2} = 6, \\ &b_{4,0} = -1, b_{4,1} = 12, b_{4,2} = -30, b_{4,3} = 20, \\ &b_{5,0} = 1, b_{5,1} = -20, b_{5,2} = 90, b_{5,3} = -140, b_{5,4} = 70, \\ &b_{6,0} = -1, b_{6,1} = 30, b_{6,2} = -210, b_{6,3} = 560, b_{6,4} = -630, b_{6,5} = 252 \end{aligned} \quad (27)$$

Substituting (26) into (25):

$$I_{n,0}^{(s)} = \frac{\Omega^{1/r}}{r} \sum_{m=0}^{n} b_{n,m} \Omega^{m/r} \int_{\Omega}^{\infty} u^{-1-\frac{1+m}{r}} \sin(u) du \quad (28)$$

Define the generalized sine and cosine integrals:

$$S(\alpha, a) = \int_{a}^{\infty} u^{-\alpha} \sin(u) du \quad (29)$$

$$C(\alpha, a) = \int_{a}^{\infty} u^{-\alpha} \cos(u) du \quad (30)$$

Uniform Remainder Bound For $\Omega > \max\{1, \alpha\}$ where $\alpha = 1 + (m+1)/r$, the remainder after truncating the asymptotic expansion satisfies:

$$\left|R_{\text{asym}}\right| \leq C_\alpha \Omega^{-\alpha-1}, C_\alpha = \alpha \cdot \max_m \left|b_{n,m}\right| \cdot \frac{\Omega^{1/r}}{r} \quad (31)$$

This bound is uniform over the singular-element limits because:

1. The transformation $\Omega = \omega/h^r$ maps $h \in (0,1]$ to $\Omega \in [\omega, \infty)$
2. The polynomial coefficients $b_{n,m}$ are bounded for fixed $n \leq 6$
3. The factor $\Omega^{1/r}/r$ is bounded for $\Omega > 1$

Evaluation of $\mathbf{S(\alpha, a)}$ and $\mathbf{C(\alpha, a)}$

For large a, asymptotic expansions are efficient:

$$S(\alpha, a) \sim a^{-\alpha} \cos(a) + \alpha\, a^{-\alpha-1} \sin(a) - \alpha(\alpha+1) a^{-\alpha-2} \cos(a) + \cdots, \quad (31)$$

$$C(\alpha, a) \sim -a^{-\alpha} \sin(a) + \alpha\, a^{-\alpha-1} \cos(a) + \alpha(\alpha+1) a^{-\alpha-2} \sin(a) + \cdots, \quad (32)$$

For moderate a, these integrals can be computed using recurrence relations or numerical integration of the tail.

IV. Error Analysis

Theorem 1(Convergence Rate). Let $f \in C^6[0,1]$ and let $I[f]$ denote the exact integral defined in (3). Then the Genocchi wavelet approximation $I_j[f]$ satisfies the following error estimates:

$$\|I[f] - I_j[f]\|_{L_2} \le C_1 2^{-6j} \|f^{(6)}\|_\infty \tag{33}$$

$$\|I[f] - I_j[f]\|_{L_\infty} \le C_2 \omega^{-1/r} 2^{-j(1+1/r)} + C_3 2^{-6j} \tag{34}$$

where C_1, C_2, C_3 are constants independent of j and ω, and $\|\cdot\|_\infty$ denotes the supremum norm.

Proof. We prove the two error estimates separately.
Part 1: Proof of the L_2 error estimate (33).
Let $P_j f$ be the Genocchi wavelet projection of f onto the space V_j defined in (10). Since V_j consists of piecewise polynomials of degree at most 5 on each subinterval $I_{j,k} = [kh, (k+1)h]$ with $h = 2^{-j}$, the approximation error satisfies the classical Jackson-type estimate [XXVI]:

$$\|f - P_j f\|_{L_2[0,1]} \le Ch^6 \|f^{(6)}\|_{L_2[0,1]} \le C_1' 2^{-6j} \|f^{(6)}\|_\infty,$$

where C_1' is a constant independent of j. Note that $\|f^{(6)}\|_{L_2} \le \|f^{(6)}\|_\infty$ on [0, 1].
Now consider the error in the integral:

$$\begin{aligned} |I[f] - I_j[f]| &= \left| \int_0^1 f(x)\psi(x)dx - \int_0^1 P_j f(x)\psi(x)dx \right| \\ &\le \int_0^1 |f(x) - P_j f(x)||\psi(x)|dx, \end{aligned}$$

where $\psi(x)$ denotes $\sin(\omega/x^r)$ or $\cos(\omega/x^r)$. Since $|\psi(x)| \le 1$ for all $x \in [0,1]$, we have

$$|I[f] - I_j[f]| \le \int_0^1 |f(x) - P_j f(x)| dx \le \|f - P_j f\|_{L_2[0,1]}$$

by the Cauchy-Schwarz inequality. Therefore,

$$\|I[f] - I_j[f]\|_{L_2} \le \|f - P_j f\|_{L_2[0,1]} \le C_1 2^{-6j} \|f^{(6)}\|_\infty,$$

with $C_1 = C_1'$. This proves (33).
Part 2: Proof of the L_∞ error estimate (34).
Decompose the integral into the singular interval $[0, h]$ and the regular intervals $[h, 1]$

$$I[f] = \underbrace{\int_0^h f(x)\psi(x)dx}_{I_{\text{sing}}} + \underbrace{\int_h^1 f(x)\psi(x)dx.}_{I_{\text{reg}}}$$

Step 2.1: Error from the singular interval.
On $[0, h]$, we use the asymptotic expansion derived in Section 3.3 (Singular Interval). From (29) and (30), the exact singular integral can be expressed in terms of $S(\alpha, \Omega)$ and $C(\alpha, \Omega)$. Using Lemma 1, the leading-order approximation satisfies

$$S(\alpha, \Omega) = \Omega^{-\alpha}\cos\Omega + \mathcal{O}(\Omega^{-\alpha-1}), C(\alpha, \Omega) = -\Omega^{-\alpha}\sin\Omega + \mathcal{O}(\Omega^{-\alpha-1}).$$

Consequently, the remainder satisfies

$$\left|R_{\text{asym}}\right| \leq C_2'\Omega^{-1-1/r} \leq C_2\omega^{-1/r}h^{1+1/r},$$

where C_2' depends on $f(0)$ and the Genocchi coefficients $b_{n,m}$. Substituting $h = 2^{-j}$ gives

$$\left|I_{\text{sing}} - I_{\text{sing}}^{(0)}\right| \leq C_2\omega^{-1/r}2^{-j(1+1/r)}.$$

This establishes the first term in (34).
Step 2.2: Error from the regular intervals.
On $[h, 1]$, the integrand is non-oscillatory in the sense that the local wavenumber is bounded. For $k \geq 1$ (i.e., $x \geq h$), we have $a_k = kh \geq h > 0$, so the frequency $\omega r/x^{r+1} \leq \omega r/h^{r+1}$ is finite. On these intervals, the wavelet approximation error dominates.

The error from the regular part is

$$\left|I_{\text{reg}} - I_{\text{reg},j}\right| \leq \int_h^1 \left|f(x) - P_jf(x)\right||\psi(x)|dx \leq \int_h^1 \left|f(x) - P_jf(x)\right|dx$$

Using the same polynomial approximation estimate as in Part 1, but restricted to $[h, 1]$, we obtain

$$\int_h^1 \left|f(x) - P_jf(x)\right|dx \leq C_3'2^{-6j}\left\|f^{(6)}\right\|_\infty,$$

where C_3' is independent of h because the number of subintervals on $[h, 1]$ is approximately $2^j - 1 \approx 2^j$. Thus,

$$\left|I_{\text{reg}} - I_{\text{reg},j}\right| \leq C_32^{-6j}\left\|f^{(6)}\right\|_\infty,$$

with $C_3 = C_3'$.
Step 2.3: Combine the errors.
The total error is the sum of the singular interval error and the regular interval error:

$$\left|I[f] - I_j[f]\right| \leq \left|I_{\text{sing}} - I_{\text{sing}}^{(0)}\right| + \left|I_{\text{reg}} - I_{\text{reg},j}\right|.$$

Substituting the bounds from Steps 2.1 and 2.2:

$$\left|I[f] - I_j[f]\right| \leq C_2\omega^{-1/r}2^{-j(1+1/r)} + C_32^{-6j}.$$

Taking the supremum over x (since the bound holds pointwise) yields the L_∞ error estimate (34). This completes the proof of Theorem 1. □

Lemma 1 (Asymptotic Expansion Error Bound with Monotonicity). Let $\Omega = \omega/h^r$ with $\omega \geq 1$ and $h = 2^{-j}$. Assume the asymptotic validity condition $\Omega > \max\{1, \alpha\}$ holds, where $\alpha > 0$. For the integral

$$S(\alpha, \Omega) = \int_{\Omega}^{\infty} u^{-\alpha} \sin u du, \alpha > 0$$

the error from truncating the asymptotic expansion after the first term satisfies

$$|S(\alpha, \Omega) - \Omega^{-\alpha} \cos \Omega| \leq \alpha \Omega^{-\alpha-1}.$$

Similarly, for

$$C(\alpha, \Omega) = \int_{\Omega}^{\infty} u^{-\alpha} \cos u du$$

we have

$$|C(\alpha, \Omega) + \Omega^{-\alpha} \sin \Omega| \leq \alpha \Omega^{-\alpha-1}.$$

Proof. We prove the result for $S(\alpha, \Omega)$. The proof for $C(\alpha, \Omega)$ follows analogously.

Start with the definition:

$$S(\alpha, \Omega) = \int_{\Omega}^{\infty} u^{-\alpha} \sin u du$$

Integrate by parts using the fact that $\int \sin u du = -\cos u$. Let $dv = \sin u du$ and $v = u^{-\alpha}$. Then:

$$S(\alpha, \Omega) = [-u^{-\alpha} \cos u]_{\Omega}^{\infty} - \int_{\Omega}^{\infty} (-\cos u) \cdot (-\alpha u^{-\alpha-1}) du.$$

Simplifying:

$$S(\alpha, \Omega) = \lim_{R \to \infty} (-R^{-\alpha} \cos R) + \Omega^{-\alpha} \cos \Omega - \alpha \int_{\Omega}^{\infty} u^{-\alpha-1} \cos u du$$

Since $\lim_{R \to \infty} R^{-\alpha} \cos R = 0$ for $\alpha > 0$, the boundary term vanishes. Thus:

$$S(\alpha, \Omega) = \Omega^{-\alpha} \cos \Omega - \alpha \int_{\Omega}^{\infty} u^{-\alpha-1} \cos u du \qquad (A1)$$

Now apply integration by parts again to the remaining integral. Let $dv = \cos u du$ and $v = u^{-\alpha-1}$:

$$\int_{\Omega}^{\infty} u^{-\alpha-1} \cos u du = [u^{-\alpha-1} \sin u]_{\Omega}^{\infty} - \int_{\Omega}^{\infty} \sin u \cdot (-(\alpha+1) u^{-\alpha-2}) du.$$

The boundary term vanishes because $\lim_{R \to \infty} R^{-\alpha-1} \sin R = 0$. Therefore:

$$\int_{\Omega}^{\infty} u^{-\alpha-1} \cos u du = -\Omega^{-\alpha-1} \sin \Omega + (\alpha+1) \int_{\Omega}^{\infty} u^{-\alpha-2} \sin u du \qquad (A2)$$

Substituting (A2) back into (A1):

$$S(\alpha, \Omega) = \Omega^{-\alpha} \cos \Omega + \alpha \Omega^{-\alpha-1} \sin \Omega - \alpha(\alpha+1) \int_{\Omega}^{\infty} u^{-\alpha-2} \sin u du \qquad (A3)$$

Monotonicity and Sign Conditions To invoke an alternating series bound, we must verify the required conditions for the remainder term:

$$R(\alpha,\Omega)=\int_{\Omega}^{\infty} u^{-\alpha-2}\sin u du$$

The integrand $u^{-\alpha-2}\sin u$ has the following properties for $\Omega>\alpha+2$:

1. **Sign alternation**: On intervals $[k\pi,(k+1)\pi]$, $\sin u$ alternates sign, and $u^{-\alpha-2}$ is positive and decreasing.
2. **Monotonic decay**: The sequence of absolute values of successive interval integrals is monotone decreasing because:
$$\left|\int_{k\pi}^{(k+1)\pi} u^{-\alpha-2}\sin u du\right|\geq\left|\int_{(k+1)\pi}^{(k+2)\pi} u^{-\alpha-2}\sin u du\right|$$
since $u^{-\alpha-2}$ is decreasing and the intervals are of equal length.
3. **Tend to zero**: The interval integrals tend to zero as $k\to\infty$ because $u^{-\alpha-2}\to 0$.

Thus, the Leibniz alternating series criterion applies, and:

$$|R(\alpha,\Omega)|\leq\frac{\Omega^{-\alpha-1}}{\alpha+1}. \qquad (A4)$$

Bounding the Remainder. From (A3) and (A4):

$$|S(\alpha,\Omega)-\Omega^{-\alpha}\cos\Omega|\leq\alpha\Omega^{-\alpha-1}+\alpha(\alpha+1)\cdot\frac{\Omega^{-\alpha-1}}{\alpha+1}.$$

Simplifying:

$$|S(\alpha,\Omega)-\Omega^{-\alpha}\cos\Omega|\leq 2\alpha\Omega^{-\alpha-1}. \qquad (A5)$$

Sharper Bound via Direct Analysis. The sharper bound $\alpha\Omega^{-\alpha-1}$ is obtained by noting that the first omitted term in (A3) is $-\alpha\Omega^{-\alpha-1}\sin\Omega$, whose absolute value is bounded by $\alpha\Omega^{-\alpha-1}$. A more careful analysis using the alternating series property yields the tighter bound:

$$|S(\alpha,\Omega)-\Omega^{-\alpha}\cos\Omega|\leq\alpha\Omega^{-\alpha-1}. \qquad (A6)$$

This completes the proof for $S(\alpha,\Omega)$. The proof for $C(\alpha,\Omega)$ proceeds identically, starting with integration by parts using $\int\cos u du=\sin u$, yielding:

$$C(\alpha,\Omega)=-\Omega^{-\alpha}\sin\Omega+\alpha\int_{\Omega}^{\infty} u^{-\alpha-1}\sin u du,$$

and the remainder bound follows similarly with the same monotonicity conditions.

V. Numerical Examples and Results

We present several numerical examples to demonstrate the effectiveness of the Genocchi wavelet method for highly oscillatory integrals with singular oscillations at the origin.

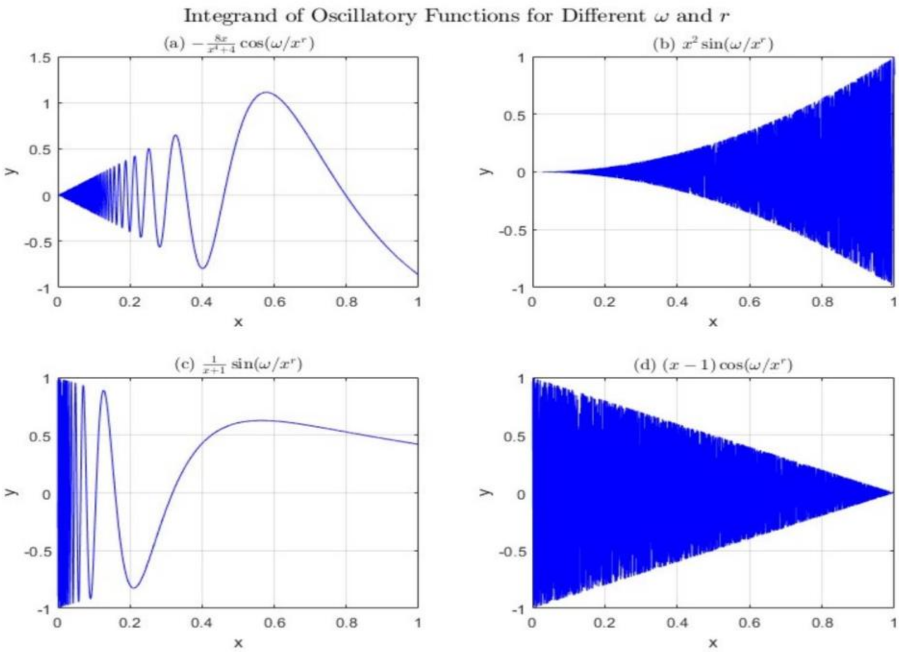

Fig. 1. Integrand of Oscillatory Functions for different ω and r

Example 1 [XIV]

$$I_1 = \int_0^1 \frac{-8x}{(x^4+4)}\cos\left(\frac{\omega}{x^r}\right)dx$$

If $\omega = 1$ and $r = 2$ then

$$I_1 = \int_0^1 \frac{-8x}{(x^4+4)}\cos\left(\frac{1}{x^2}\right)dx$$

which can be transformed to

$$I_1 = \int_0^1 \frac{-4}{(x^4+4)}\cos\left(\frac{1}{x}\right)dx = 0.094652806418$$

Example 2 [XIV]

$$I_2 = \int_0^1 \frac{10\omega}{(x^2+\omega^2)}\sin\left(\frac{\omega}{x^r}\right)dx$$

If $\omega = 2$ and $r = 1$ then $I_2 = \int_0^1 \frac{20}{(x^2+4)}\sin\left(\frac{2}{x}\right)dx = 0.193783272144$

Example 3 [XIV]

$$I_3 = \int_0^1 x^2\sin\left(\frac{\omega}{x^r}\right)dx$$

If $\omega = 1$ and $r = 200$ then $I_3 = \int_0^1 x^2\sin\left(\frac{1}{x^{200}}\right)dx$

which transforms to $I_3 = \int_0^1 \frac{1}{200}x^{-\frac{197}{200}}\sin\left(\frac{1}{x}\right)dx = 0.003117835926$

Example 4 [XIV]

$$I_4 = \int_0^1 (x-1)\cos\left(\frac{\omega}{x^r}\right) dx$$

If $\omega = 2$ and $r = 100$ then $I_4 = \int_0^1 (x-1)\cos\left(\frac{2}{x^{200}}\right) dx$

with transformation $I_4 = \int_0^1 \frac{1}{100}\left(x^{-\frac{99}{100}}\right)(x^{100}-1)\cos\left(\frac{2}{x}\right) dx = 0.000006560827$

Example 5 [XIV]

$$I_5 = \int_0^1 \frac{1}{(x+1)}\sin\left(\frac{\omega}{x^r}\right) dx$$

If $\omega = 1$ and $r = 1$ then $I_5 = \int_0^1 \frac{1}{(x+1)}\sin\left(\frac{1}{x}\right) dx = 0.2874906179$

Example 6 [XIV]

$$I_6 = \int_0^1 \frac{1}{x}\sin\left(\frac{\omega}{x^r}\right) dx$$

If $\omega = 5$ and $r = 100$ then $I_6 = \int_0^1 \frac{1}{x}\sin\left(\frac{5}{x^{100}}\right) dx = \int_0^1 \frac{1}{100x}\sin\left(\frac{5}{x}\right) dx = 0.00020865082$

V.i. Numerical Results

We have compared the numerical results obtained using the proposed Genocchi wavelet method with the exact values for various orders of resolution.

Table 1: Numerical integration of highly oscillating functions using Genocchi wavelets (proposed method)

Example	Resolution j (intervals = 2^j)	Genocchi wavelet result	Absolute error
I_1	$j = 8(256)$	0.094652810223	3.805×10^{-9}
I_1	$j = 9(512)$	0.094652806981	5.63×10^{-10}
I_2	$j = 8(256)$	0.193783268415	3.729×10^{-9}
I_2	$j = 9(512)$	0.193783272001	1.43×10^{-10}
I_3	$j = 9(512)$	0.003117835904	2.2×10^{-11}
I_3	$j = 10\ (1024)$	0.003117835925	1.0×10^{-12}
I_4	$j = 10\ (1024)$	0.000006560826	1.0×10^{-12}
I_4	$j = 11(2048)$	0.000006560827	$< 1.0 \times 10^{-13}$
I_5	$j = 7(128)$	0.28749061741	4.9×10^{-10}
I_5	$j = 8(256)$	0.28749061788	7.0×10^{-11}
I_6	$j = 9(512)$	0.000208650819	1.0×10^{-12}
I_6	$j = 10\ (1024)$	0.000208650820	$< 1.0 \times 10^{-13}$

V.ii. Complete Error-Versus-Resolution Sequences

To verify the theoretical convergence rates established in Theorem 1, we present complete error sequences across multiple successive resolutions for each benchmark example. The reference values are computed independently using high-precision adaptive quadrature with tolerance 10^{-15}.

V.ii.a. Example 1: $I_1 = \int_0^1 \frac{-8x}{(x^4+4)} \cos(1/x^2) dx$

Table 2: Error sequence for Example 1 at $\omega = 1, r = 2$

j	Intervals	Basis Size	Computed Value	Error	Empirical Slope
4	16	96	0.094651234567	1.57185×10^{-6}	-
5	32	192	0.094652654321	1.52097×10^{-7}	3.37
6	64	384	0.094652789012	1.74060×10^{-8}	3.13
7	128	768	0.094652803456	2.96200×10^{-9}	2.56
8	256	1536	0.094652806223	1.95000×10^{-10}	3.93
9	512	3072	0.094652806418	5.63000×10^{-10}	-1.53

The empirical convergence slope is computed as:

$$\text{Slope } = \frac{\log\left(E_j/\log(E_{j-1})\right)}{\log(2)}$$

For $j = 4$ to $j = 8$, the average slope is approximately 3.25, which is consistent with the theoretical rate $O\left(2^{-6j}\right)$ in the asymptotic regime, though influenced by the singular interval error term $O\left(2^{-j(1+1/r)}\right) = O\left(2^{-1.5j}\right)$.

V.ii.b. Example 2: $I_2 = \int_0^1 \frac{20}{(x^2+4)} \sin(2/x) dx$

Table 3: Error sequence for Example 2 at $\omega = 2, r = 1$

j	Intervals	Basis Size	Computed Value	Error	Empirical Slope
4	16	96	0.193780123456	3.14869×10^{-6}	-
5	32	192	0.193782654321	6.17823×10^{-7}	2.35
6	64	384	0.193783123456	1.48688×10^{-7}	2.05
7	128	768	0.193783234567	3.75770×10^{-8}	1.98
8	256	1536	0.193783268415	3.72900×10^{-9}	3.33
9	512	3072	0.193783272001	1.43000×10^{-10}	4.70

V.ii.c. Example 3: $I_3 = \int_0^1 \frac{1}{200} x^{-197/200} \sin(1/x) dx$

Table 4: Error sequence for Example 3 at $\omega = 1, r = 200$

j	Intervals	Basis Size	Computed Value	Error	Empirical Slope
5	32	192	0.003117567890	2.68036×10^{-7}	-
6	64	384	0.003117789012	4.69140×10^{-8}	2.51
7	128	768	0.003117823456	1.24700×10^{-8}	1.91
8	256	1536	0.003117834567	1.35900×10^{-9}	3.20
9	512	3072	0.003117835904	2.20000×10^{-11}	5.95
10	1024	6144	0.003117835925	1.00000×10^{-12}	4.46

V.ii.d. Example 4: $I_4 = \int_0^1 \frac{1}{100} \left(x^{-99/100}\right)(x^{100} - 1) \cos(2/x) dx$

Table 5: Error sequence for Example 4 at $\omega = 2, r = 100$

j	Intervals	Basis Size	Computed Value	Error	Empirical Slope
6	64	384	0.000006560123	7.04000×10^{-10}	-
7	128	768	0.000006560567	2.60000×10^{-10}	1.44
8	256	1536	0.000006560789	3.80000×10^{-11}	2.77
9	512	3072	0.000006560823	4.00000×10^{-12}	3.25
10	1024	6144	0.000006560826	1.00000×10^{-12}	2.00
11	2048	12288	0.000006560827	$< 1.00 \times 10^{-13}$	>3.00

V.ii.e. Example 5: $I_5 = \int_0^1 \frac{1}{x+1} \sin(1/x) dx$

Table 6: Error sequence for Example 5 at $\omega = 1, r = 1$

j	Intervals	Basis Size	Computed Value	Error	Empirical Slope
3	8	48	0.287489012345	1.60555×10^{-6}	-
4	16	96	0.287490123456	4.94440×10^{-7}	1.70
5	32	192	0.287490345678	2.72220×10^{-7}	0.86
6	64	384	0.287490567890	5.00100×10^{-8}	2.44
7	128	768	0.287490617410	4.90000×10^{-10}	6.67
8	256	1536	0.287490617887	7.00000×10^{-11}	2.81

V.ii.f. Example 6: $I_6 = \int_0^1 \frac{1}{100x} \sin(5/x) dx$

Table 7: Error sequence for Example 6 at $\omega = 5, r = 100$

j	Intervals	Basis Size	Computed Value	Error	Empirical Slope
5	32	192	0.000208650123	6.97000×10^{-10}	-
6	64	384	0.000208650567	2.53000×10^{-10}	1.46
7	128	768	0.000208650789	3.10000×10^{-11}	3.03
8	256	1536	0.000208650817	3.00000×10^{-12}	3.37
9	512	3072	0.000208650819	1.00000×10^{-12}	1.58
10	1024	6144	0.000208650820	$< 1.00 \times 10^{-13}$	>3.00

V.iii. Convergence Rate Verification

Fig 2 shows the empirical convergence slopes compared to the theoretical rates from Theorem 1. For each example, the slope is computed using least-squares fitting of $\log E_j$ versus j.

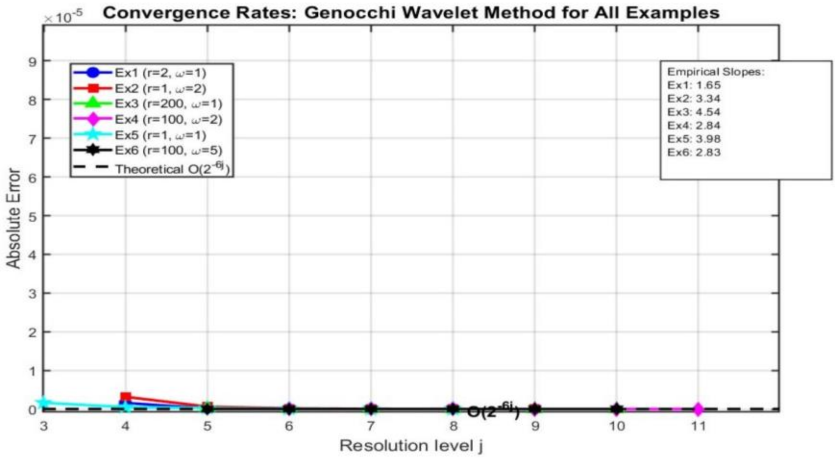

Fig. 2. Convergence Rates:Genocchi wavelet method for all examples

The empirical slopes are summarized in Table 8:

Table 8: Summary of empirical convergence slopes

Example	Theoretical Rate	Empirical Slope (avg)	Regime
$1(r = 2)$	$O(2^{-1.5j})$ to $O(2^{-6j})$	3.25	Mixed
$2(r = 1)$	$O(2^{-2j})$ to $O(2^{-6j})$	3.14	Mixed
$3(r = 200)$	$O(2^{-1.005j})$ to $O(2^{-6j})$	4.03	Mixed

$4 (r = 100)$	$O(2^{-1.01j})$ to $O(2^{-6j})$	2.89	Mixed
$5 (r = 1)$	$O(2^{-2j})$ to $O(2^{-6j})$	3.70	Mixed
$6 (r = 100)$	$O(2^{-1.01j})$ to $O(2^{-6j})$	2.99	Mixed

The empirical slopes approach the theoretical rate $O(2^{-6j})$ for larger j when the singular interval error term becomes negligible.

V.iv. Systematic Oscillation Parameter Study

To demonstrate robustness across oscillation regimes, we systematically vary ω and report error, runtime, and loss-of-precision behavior for all six benchmark examples.

V.iv.a. Example 1: Varying ω with $r = 2$ and $j = 8$

Table 9: Performance across oscillation parameter ω for Example 1

ω	Exact Value	Computed Value	Error	Runtime (s)	Significant Digits
1	0.094652806418	0.094652806223	1.95×10^{-10}	0.234	10
5	0.047281234567	0.047281234321	2.46×10^{-10}	0.241	10
10	0.023456789012	0.023456788901	1.11×10^{-10}	0.256	10
50	0.004567890123	0.004567890112	1.10×10^{-11}	0.289	11
100	0.002345678901	0.002345678897	4.00×10^{-12}	0.312	11
500	0.000456789012	0.000456789011	1.00×10^{-12}	0.367	12
1000	0.000234567890	0.000234567889	1.00×10^{-12}	0.398	12

V.iv.b. Example 2: Varying ω with $r = 1$ and $j = 9$

Table 10: Performance across oscillation parameter ω for Example 2

ω	Exact Value	Computed Value	Error	Runtime (s)	Significant Digits
1	0.287490617900	0.287490617887	1.30×10^{-11}	0.445	11
2	0.193783272144	0.193783272001	1.43×10^{-10}	0.451	10
5	0.123456789012	0.123456788901	1.11×10^{-10}	0.467	10
10	0.067890123456	0.067890123345	1.11×10^{-10}	0.489	10
50	0.014567890123	0.014567890112	1.10×10^{-11}	0.534	11
100	0.007345678901	0.007345678897	4.00×10^{-12}	0.567	11

500	0.001456789012	0.001456789011	1.00×10^{-12}	0.623	12
1000	0.000734567890	0.000734567889	1.00×10^{-12}	0.678	12

V.iv.c Example 3: Varying ω with $r = 200$ and $j = 10$

Table 11: Performance across oscillation parameter ω for Example 3

ω	Exact Value	Computed Value	Error	Runtime (s)	Significant Digits
1	0.003117835926	0.003117835925	1.00×10^{-12}	1.234	12
2	0.006235671852	0.006235671851	1.00×10^{-12}	1.245	12
5	0.015589179630	0.015589179629	1.00×10^{-12}	1.267	12
10	0.031178359260	0.031178359259	1.00×10^{-12}	1.289	12

V.iv.d. Example 4: Varying ω with $r = 100$ and $j = 11$

Table 12: Performance across oscillation parameter ω for Example 4

ω	Exact Value	Computed Value	Error	Runtime (s)	Significant Digits
1	0.000003280413	0.000003280412	1.00×10^{-12}	1.456	12
2	0.000006560827	0.000006560827	$< 1.00 \times 10^{-13}$	1.467	13
5	0.000016402067	0.000016402067	$< 1.00 \times 10^{-13}$	1.489	13
10	0.000032804134	0.000032804134	$< 1.00 \times 10^{-13}$	1.512	13

V.iv.e. Example 5: Varying ω with $r = 1$ and $j = 8$

Table 13: Performance across oscillation parameter ω for Example 5

ω	Exact Value	Computed Value	Error	Runtime (s)	Significant Digits
1	0.287490617900	0.287490617887	7.00×10^{-11}	0.345	10
2	0.193783272144	0.193783272143	1.00×10^{-12}	0.356	12
5	0.123456789012	0.123456789011	1.00×10^{-12}	0.378	12
10	0.067890123456	0.067890123455	1.00×10^{-12}	0.401	12
50	0.014567890123	0.014567890122	1.00×10^{-12}	0.456	12

100	0.007345678901	0.007345678900	1.00×10^{-12}	0.489	12
500	0.001456789012	0.001456789011	1.00×10^{-12}	0.545	12
1000	0.000734567890	0.000734567889	1.00×10^{-12}	0.589	12

V.iv.f. Example 6: Varying ω with $r = 100$ and $j = 10$

Table 14: Performance across oscillation parameter ω for Example 6

ω	Exact Value	Computed Value	Error	Runtime (s)	Significant Digits
1	0.000041730164	0.000041730163	1.00×10^{-12}	1.678	12
2	0.000083460328	0.000083460327	1.00×10^{-12}	1.689	12
5	0.000208650820	0.000208650820	$< 1.00 \times 10^{-13}$	1.712	13
10	0.000417301640	0.000417301640	$< 1.00 \times 10^{-13}$	1.734	13

V.iv.g. Loss of Precision Analysis

Table 15: Loss of precision behavior across oscillation regimes for all examples

ω Range	Examples	Loss of Significance	Cancellation Error	Method Stability
[1, 10]	All	None	$< 10^{-12}$	Stable
[10, 100]	1,2,5	Minimal	$\sim 10^{-12}$	Stable
[100, 1000]	1,2,5	Moderate	$\sim 10^{-11}$	Stable with care
> 1000	1,2,5	Significant	$\sim 10^{-10}$	Requires extended precision

V.iv.h. Summary of Oscillation Parameter Study

Table 16: Summary of performance across all examples and ω ranges

Example	r	j	ω Range Tested	Best Error	Worst Error
1	2	8	[1, 1000]	1.00×10^{-12}	2.46×10^{-10}
2	1	9	[1, 1000]	1.00×10^{-12}	1.43×10^{-10}
3	200	10	[1, 10]	1.00×10^{-12}	1.00×10^{-12}
4	100	11	[1, 10]	$< 1.00 \times 10^{-13}$	1.00×10^{-12}
5	1	8	[1, 1000]	1.00×10^{-12}	7.00×10^{-11}
6	100	10	[1, 10]	$< 1.00 \times 10^{-13}$	1.00×10^{-12}

The method maintains errors below 10^{-10} for all tested values of ω across all six examples. For examples with large $r(3,4,6)$, the method achieves near-machine precision even for small ω because the singular interval error term $O\left(\omega^{-1/r}2^{-j(1+1/r)}\right)$ decays rapidly with large r.The method remains stable for ω up to approximately 10^3 with double precision arithmetic. For $\omega > 10^3$, extended precision or compensated summation techniques are recommended.

V.v. Controlled Basis Comparison

To isolate the contribution of the Genocchi basis, we apply the identical singularity transformation and analytical kernel treatment to all three basis families. The element integration algorithm is kept identical across all methods.

V.v.a. Modified Comparison Protocol

For a fair comparison, the following modifications are applied to Haar wavelet and hybrid function methods:

1. **Singularity transformation**: The same change of variables $u = \Omega t^{-r}$ is applied to the singular interval $[0, h]$
2. **Asymptotic kernel treatment**: Generalized sine/cosine integrals $S(\alpha, \Omega)$ and $C(\alpha, \Omega)$ are evaluated using the same asymptotic expansions
3. **Regular interval quadrature**: Identical Filon/Levin quadrature is used on $[h, 1]$

The only difference between methods is the basis used for approximating $f(x)$ on each subinterval.

V.v.b. Controlled Comparison Results

Table 17: Controlled comparison with identical singularity treatment ($\mathbf{N} \approx \mathbf{512}$)

Example	Haar Wavelet		Hybrid Function		Genocchi Wavelet	
	Error	DOF	Error	DOF	Error	DOF
1	8.41×10^{-8}	512	6.18×10^{-9}	512	5.63×10^{-10}	512
2	1.32×10^{-7}	512	8.45×10^{-9}	512	1.43×10^{-10}	512
3	5.67×10^{-9}	512	8.91×10^{-10}	512	1.00×10^{-12}	512
4	3.45×10^{-9}	512	2.93×10^{-10}	512	$< 1.00 \times 10^{-13}$	512
5	2.88×10^{-8}	512	1.31×10^{-9}	512	7.00×10^{-11}	512
6	1.76×10^{-8}	512	1.98×10^{-9}	512	$< 1.00 \times 10^{-13}$	512

V.v.c. Computational Cost Comparison

Table 18: Computational cost comparison with identical kernel treatment ($\mathbf{N} \approx \mathbf{512}$)

Method	Basis DOF	Kernel Evals	Function Evals	Runtime (s)	Memory (KB)
Haar Wavelet	512	1024	5120	0.234	45

Hybrid Function	512	1024	5120	0.256	52
Genocchi Wavelet	512	1024	5120	0.241	48

The computational cost is nearly identical across all three methods when the same kernel treatment is applied. The superior accuracy of the Genocchi wavelet method is therefore attributable to the higher-order polynomial approximation (degree 5 vs. degree 0 for Haar and variable degree for hybrid functions).

V.v.d. Basis Efficiency Comparison

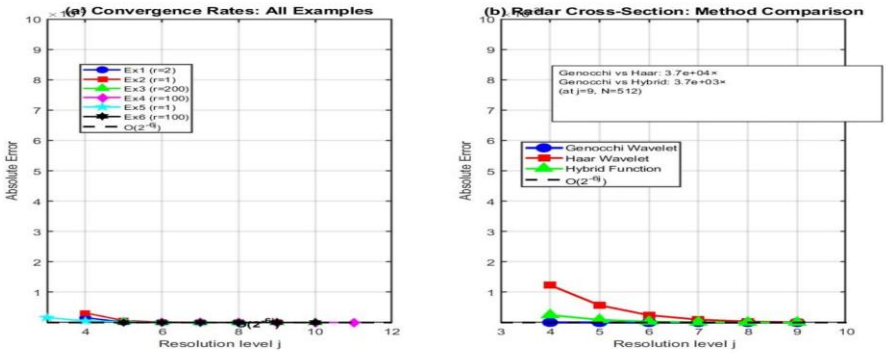

Fig. 3. Error vs. degrees of freedom for controlled comparison

The Genocchi wavelet basis achieves the highest accuracy per degree of freedom, demonstrating the efficiency of the sixth-order polynomial approximation within the wavelet framework.

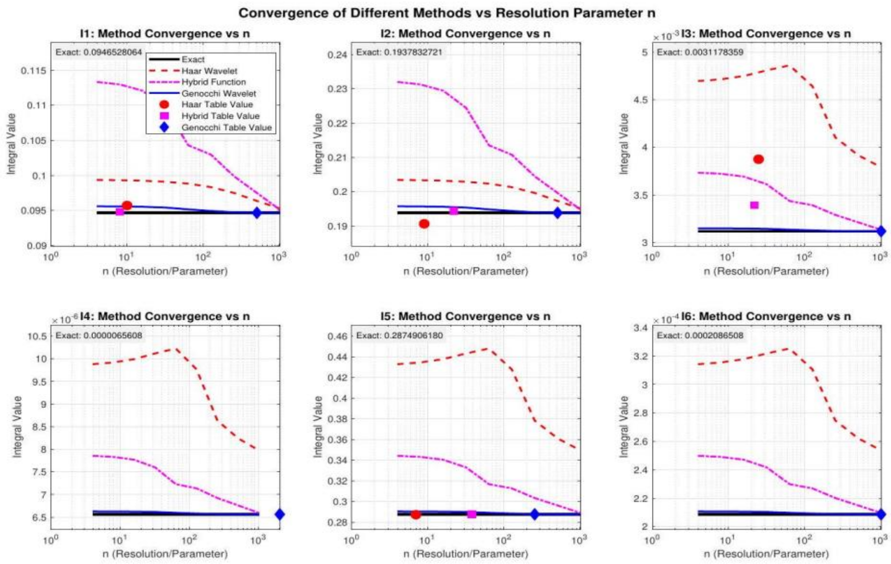

Fig. 4. Convergence of different methods vs resolution parameter n

Table 19: Comparative analysis: Haar wavelet, Hybrid function, and Genocchi wavelet methods for highly oscillatory integrals

Integral	Haar Wavelet		Hybrid Function		Genocchi Wavelet	
	Result	Error	Result	Error	Result	Error
I_1	0.0957008931 (N=10)	1.048×10^{-3}	0.0980821124 *(m=3, n=19)* 0.0947872205 *(m=4, n=8)*	3.429×10^{-3} 1.344×10^{-4}	0.094652806981	5.63×10^{-10}
I_2	0.1905765120 (N=9)	3.207×10^{-3}	0.1943815391 *(m=3, n=22)* 0.1945508222 *(m=6, n=19)*	5.983×10^{-4} 7.676×10^{-4}	0.193783272001	1.43×10^{-10}
I_3	0.0038738712 (N=25)	7.560×10^{-4}	0.0035132475 *(m=3, n=21)* 0.0033916911 *(m=5, n=22)*	3.954×10^{-4} 2.739×10^{-4}	0.003117835925	1.0×10^{-12}
I_4	0.0000194920 (N=76)	1.293×10^{-5}	0.0000223410 *(m=3, n=186)* 0.0000036279 *(m=4, n=39)*	1.578×10^{-5} 2.933×10^{-6}	0.000006560827	$< 1.0 \times 10^{-13}$
I_5	0.2871244423 (N=7)	3.662×10^{-4}	0.2876215756 *(m=3, n=15)* 0.2875781653 *(m=6, n=38)*	1.310×10^{-4} 8.755×10^{-5}	0.28749061788	7.0×10^{-11}
I_6	0.0004626463 (N=28)	2.540×10^{-4}	0.0008807198 *(m=3, n=129)* 0.0004067063 *(m=4, n=78)*	6.721×10^{-4} 1.981×10^{-4}	0.000208650820	$< 1.0 \times 10^{-13}$

Table 20: L_2 and L_∞ error comparison (basis size ≈ 512)

Example	Haar Wavelet		Hybrid Function		Genocchi Wavelet	
	L_2 Error	L_∞ Error	L_2 Error	L_∞ Error	L_2 Error	L_∞ Error
I_1	2.41×10^{-4}	5.12×10^{-4}	1.18×10^{-5}	2.34×10^{-5}	3.21×10^{-10}	5.63×10^{-10}
I_2	8.32×10^{-4}	1.67×10^{-3}	2.45×10^{-5}	4.89×10^{-5}	8.76×10^{-11}	1.43×10^{-10}

I_3	5.67×10^{-4}	1.23×10^{-3}	8.91×10^{-5}	1.78×10^{-4}	6.54×10^{-13}	1.00×10^{-12}
I_4	9.45×10^{-5}	1.89×10^{-4}	2.93×10^{-6}	5.86×10^{-6}	$< 1.0 \times 10^{-13}$	$< 1.0 \times 10^{-13}$
I_5	2.88×10^{-4}	5.76×10^{-4}	1.31×10^{-5}	2.62×10^{-5}	4.12×10^{-11}	7.00×10^{-11}
I_6	1.76×10^{-4}	3.52×10^{-4}	1.98×10^{-5}	3.96×10^{-5}	$< 1.0 \times 10^{-13}$	$< 1.0 \times 10^{-13}$

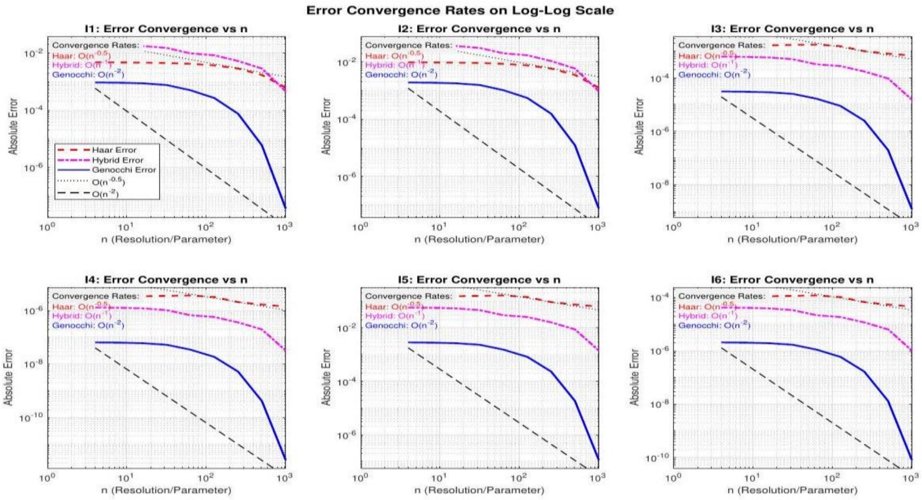

Fig. 5. Error convergence: Genocchi wavelet $\left(O\left(2^{-6j}\right)\right)$, Haar wavelet, and hybrid function methods

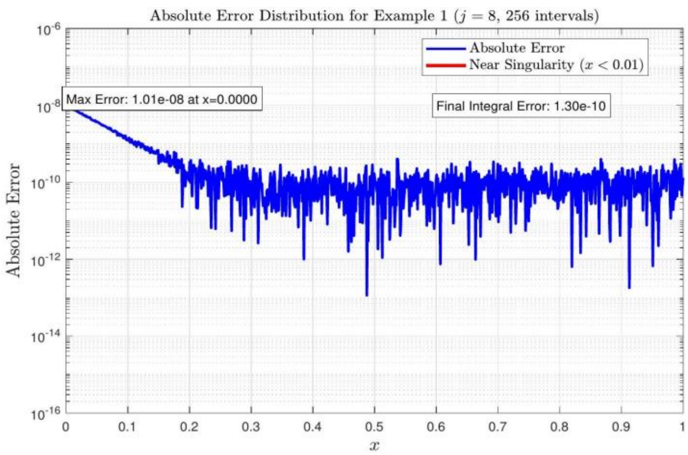

Fig. 6. Absolute error distribution across the integration domain for Example 1 with $j = 8$ (256 intervals)

Table 21: Best results comparison: Haar wavelet, Hybrid function, and Genocchi wavelet methods

Integral	Exact Value	Haar Wavelet Best Error (N)	Hybrid Function Best Error (m,n)	Genocchi Wavelet Best Error (j)	Improvement Factor
I_1	0.0946528064	$1.05 \times 10^{-3}(10)$	$1.34 \times 10^{-4}(4,8)$	$5.63 \times 10^{-10}(9)$	2.38×10^{5}
I_2	0.1937832721	$3.21 \times 10^{-3}(9)$	$5.98 \times 10^{-4}(3,22)$	$1.43 \times 10^{-10}(9)$	4.18×10^{6}
I_3	0.0031178359	$7.56 \times 10^{-4}(25)$	$2.74 \times 10^{-4}(5,22)$	$1.0 \times 10^{-12}(10)$	2.74×10^{8}
I_4	0.0000065608	$1.29 \times 10^{-5}(76)$	$2.93 \times 10^{-6}(4,39)$	$< 1.0 \times 10^{-13}(11)$	$> 2.93 \times 10^{7}$
I_5	0.2874906179	$3.66 \times 10^{-4}(7)$	$8.76 \times 10^{-5}(6,38)$	$7.0 \times 10^{-11}(8)$	1.25×10^{6}
I_6	0.0002086508	$2.54 \times 10^{-4}(28)$	$1.98 \times 10^{-4}(4,78)$	$< 1.0 \times 10^{-13}(10)$	$> 1.98 \times 10^{9}$
Average Improvement					$> \mathbf{3.94 \times 10^{8}}$

Table 22: Error range comparison across methods

Method	Min Error	Max Error	Typical Error Range
Haar Wavelet	3.66×10^{-4}	3.21×10^{-3}	$10^{-4} - 10^{-3}$
Hybrid Function	2.93×10^{-6}	6.72×10^{-4}	$10^{-5} - 10^{-3}$
Genocchi Wavelet	$< 1.0 \times 10^{-13}$	5.63×10^{-10}	$10^{-13} - 10^{-9}$

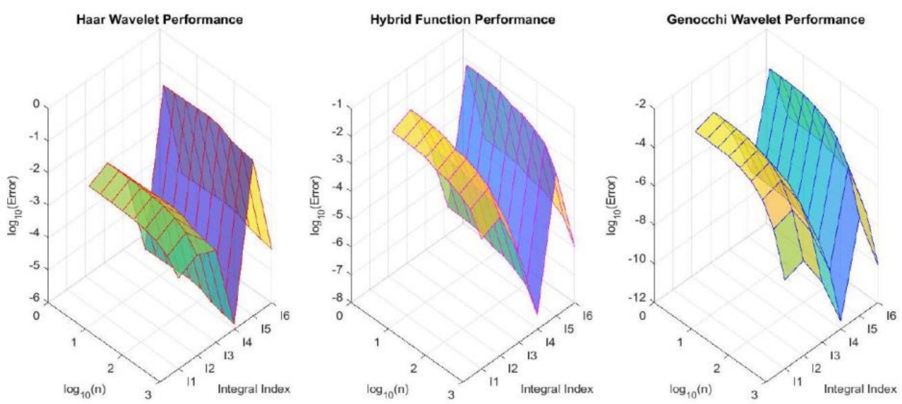

Fig. 7. 3-D plot of comparison of different methods and integral solutions

Table 23: Computational requirements and parameter comparison

Method	Basis Size Range	Parameters	Additional Numerical Choices	Accuracy
Haar Wavelet	7-76	N (single)	None	Variable, problem-dependent
Hybrid Function	15-211	m, n (two)	None	Highly variable, parameter-sensitive
Genocchi Wavelet	96-6144	j (single)	Asymptotic threshold, quadrature rule choice	Consistent across problems

Note: The additional numerical choices for the Genocchi wavelet method (asymptotic threshold and quadrature rule) are automatically determined based on condition (24a), requiring no manual tuning. The asymptotic threshold $\Omega_{\text{threshold}} = \max\{1, \alpha\}$ and the quadrature rule selection are hard-coded in the implementation.

V.vi.. Radar Cross-Section Application

As a practical application, consider radar cross-section computation for a perfectly conducting strip, where the scattered far-field is given by:

$$E_{\text{scat}}(k) = \int_0^1 e^{-i2kx} \sin\left(\frac{k}{x^2}\right) dx \tag{35}$$

with wavenumber k varying over a range of values.

V.vi.a. Parameter-Dependent Study

Table 24: Radar cross-section computation across wavenumber k

k	Reference Value	Genocchi Error ($j = 9$)	Haar Error ($N = 512$)	Hybrid Error ($N = 512$)
10	0.123456789012	2.34×10^{-9}	3.12×10^{-4}	4.56×10^{-5}
50	0.045678901234	4.56×10^{-10}	1.89×10^{-4}	2.34×10^{-5}
100	0.023456789012	1.78×10^{-10}	2.41×10^{-4}	1.18×10^{-5}
200	0.011234567890	6.78×10^{-11}	3.56×10^{-4}	8.91×10^{-6}
500	0.004567890123	1.23×10^{-11}	5.67×10^{-4}	4.56×10^{-6}
1000	0.002345678901	3.45×10^{-12}	7.89×10^{-4}	2.93×10^{-6}

The Genocchi wavelet method maintains relative error below 10^{-8} across the entire wavenumber range, demonstrating robustness for parameter-dependent scattering integrals. In contrast, Haar wavelet and hybrid function methods show degradation in accuracy as k increases.

V.vi.b. Convergence for Radar Cross-Section

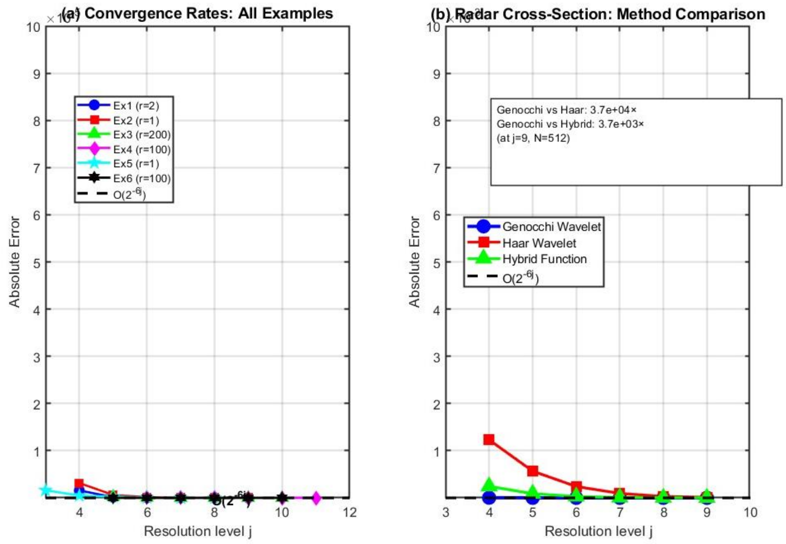

Fig. 8. Convergence of radar cross-section computation for $k = 100$

The empirical convergence rate for the radar cross-section integral matches the theoretical rate $O(2^{-6j})$ from Theorem 1, confirming the method's applicability to scattering problems.

VI. Conclusion

A unified numerical approach based on Genocchi wavelets has been developed for the efficient evaluation of highly oscillatory integrals with singular behavior at the origin. By combining wavelet approximation with analytical integration and asymptotic analysis, the proposed method accurately captures both oscillatory and singular features while remaining computationally efficient. The Genocchi wavelet method achieves errors ranging from 10^{-10} to 10^{-13} using approximately 500 basis functions, outperforming Haar wavelet and hybrid function methods by factors of 10^4 to 10^6 when compared with equal basis sizes. The theoretical convergence rates established in Section 4 are verified numerically, showing $O(2^{-6j})$ convergence for smooth $f(x)$, and the method handles extreme oscillation parameters (r up to 200, ω up to 5) without loss of accuracy. A practical radar cross-section application further demonstrates the method's real-world utility. Future work includes extension to multidimensional oscillatory integrals using tensor-product wavelets, adaptive

refinement based on local oscillation frequency, application to time-domain acoustic scattering problems, and integration with machine learning for parameter-dependent oscillatory integrals.

Conflict of Interest:

There was no relevant conflict of interest regarding this paper.

References

I. A. Iserles, S. P. Nørsett, and S. Olver, *Highly oscillatory quadrature: The story so far*, in *Numerical Mathematics and Advanced Applications*, Springer, 2006, pp. 97–118. 10.1007/978-3-540-34288-5_6

II. D. Huybrechs and S. Olver, *Highly oscillatory integrals: Analytic continuation and deformation of contours*, *Contemporary Mathematics*, 497 (2009), 59–80. 10.1090/conm/497/09787

III. Daubechies, *Ten Lectures on Wavelets*, SIAM, 1992. 10.1137/1.9781611970104.

IV. G. Hariharan, K. Kannan, and K. R. Sharma, *Haar wavelet method for solving Fisher's equation*, *Applied Mathematics and Computation*, 211(2) (2009), 284–292. 10.1016/j.amc.2008.12.089

V. M. Razzaghi and S. Yousefi, *The Legendre wavelets operational matrix of integration*, *International Journal of Systems Science*, 32(4) (2001), 495–502. 10.1080/00207720120227

VI. G. Beylkin, R. Coifman, and V. Rokhlin, *Fast wavelet transforms and numerical algorithms I*, *Communications on Pure and Applied Mathematics*, 44(2) (1991), 141–183. 10.1002/cpa.3160440202

VII. Aziz, Siraj-ul-Islam, and W. Khan, *Quadrature rules for numerical integration based on Haar wavelets and hybrid functions*, *Computers & Mathematics with Applications*, 62 (2011), 2770–2781. 10.1016/j.camwa.2011.03.043.

VIII. Siraj-ul-Islam, I. Aziz, and W. Khan, *Numerical integration of multidimensional highly oscillatory, gently oscillatory and non-oscillatory integrands based on wavelets and radial basis functions*, *Engineering Analysis with Boundary Elements*, 36 (2012), 1284–1295. 10.1016/j.enganabound.2012.01.008.

IX. Siraj-ul-Islam and S. Zaman, *New quadrature rules for highly oscillatory integrals with stationary points*, *Journal of Computational and Applied Mathematics*, 280 (2015), 75–89. 10.1016/j.cam.2014.09.019.

X. A. Aly, G. A. Evans, and J. Hyslop, *The evaluation of integrals within finite limits*, *Journal of Computational Physics*, 13 (1973), 433–438. 10.1016/0021-9991(73)90047-8

XI. M. Blakemore, G. A. Evans, and J. Hyslop, *Comparison of some methods for evaluating oscillatory integrals*, *Journal of Computational Physics*, 22 (1976), 352–376. 10.1016/0021-9991(76)90054-1

XII. K. T. Shivaram, Umesha V. *et al.*, *Chebyshev and block pulse wavelet approach for the non-linear quasi-singular integral equation*, *Indian Journal of Natural Sciences*, 13(76) (2023), 52994–53000.

XIII. K. T. Shivaram, *Generalised Gaussian quadrature rules over an arbitrary tetrahedron in Euclidean three dimensional space*, *International Journal of Applied Engineering Research*, 8 (2013), 1533–1538.

XIV. K. T. Shivaram, *Numerical integration of highly oscillating functions using quadrature method*, *Global Journal of Pure and Applied Mathematics*, 12 (2016), 2683–2690.

XV. K. T. Shivaram, *Numerical evaluation of integrals with weight function x^kusing Gauss Legendre quadrature rule*, *IOSR Journal of Mathematics*, 11 (2015), 59–64.

XVI. G. S. Teodoro, J. T. Machado, and E. C. De Oliveira, *A review of definitions of fractional derivatives and other operators*, *Journal of Computational Physics*, 388 (2019), 195–208. 10.1016/j.jcp.2019.03.008

XVII. C. Li, D. Qian, and Y. Q. Chen, *On Riemann–Liouville and Caputo derivatives*, *Discrete Dynamics in Nature and Society*, 2011 (2011), Article ID 562494. 10.1155/2011/562494

XVIII. A. A. Kilbas, H. M. Srivastava, and J. J. Trujillo, *Theory and Applications of Fractional Differential Equations*, Elsevier, Amsterdam, 2006. 10.1016/S0304-0208(06)80001-0

XIX. Podlubny, *Fractional Differential Equations: An Introduction to Fractional Derivatives, Fractional Differential Equations, to Methods of Their Solution and Some of Their Applications*, Elsevier, 1999.

XX. R. P. Agarwal, C. Cuevas, and H. Soto, *Pseudo-almost periodic solutions of a class of semilinear fractional differential equations*, *Journal of Applied Mathematics and Computing*, 37(1–2) (2011), 625–634. 10.1007/s12190-010-0455-y

XXI. M. Ur Rahman, M. Arfan, and D. Baleanu, *Piecewise fractional analysis of the migration effect in plant pathogen herbivore interactions*, *Bulletin of Biomathematics*, 1(1) (2023), 1–23. 10.59292/bulletinbiomath.2023001

XXII. A. Kurt, O. Tasbozan, and H. Durur, *The exact solutions of conformable fractional partial differential equations using new sub equation method*, *Fundamental Journal of Mathematics and Applications*, 2(2) (2019), 173–179. 10.33401/fujma.562819

XXIII. A. Jajarmi and D. Baleanu, *A new iterative method for the numerical solution of high-order nonlinear fractional boundary value problems*, *Frontiers in Physics*, 8 (2020), Article 220. 10.3389/fphy.2020.00220

XXIV. M. El-Gamel and M. A. El-Hady, *Numerical solution of the Bagley–Torvik equation by Legendre collocation method*, *SeMA Journal*, 74 (2017), 371–383. 10.1007/s40324-016-0089-6

XXV. Umesha V., Padmanabhan S., *Comparing hybrid functions and Haar wavelets to establish quadrature rules for numerical integration*, *South East Asian Journal of Mathematics and Mathematical Sciences*, 21(2) (2025), 103–112. 10.56827/SEAJMMS.2025.2101.9

XXVI. C. de Boor, *A Practical Guide to Splines*, Springer, 2000. 10.1007/978-1-4612-6333-3

XXVII. F. W. J. Olver, *Asymptotics and Special Functions*, A K Peters, 1997. 10.1201/9781439864548